MIT Open Access Articles

Improving the Simulation of the West African Monsoon Using the MIT Regional Climate Model

Massachusetts Institute of Technology

Improving the Simulation of the West African Monsoon Using the MIT Regional Climate Model

EUN-SOON IM

Singapore–MIT Alliance for Research and Technology, Center for Environmental Sensing and Modeling, Singapore

REBECCA L. GIANOTTI AND ELFATIH A. B. ELTAHIR

Ralph M. Parsons Laboratory, Massachusetts Institute of Technology, Cambridge, Massachusetts

ABSTRACT

This paper presents an evaluation of the performance of the Massachusetts Institute of Technology (MIT) regional climate model (MRCM) in simulating the West African monsoon. The MRCM is built on the Regional Climate Model, version 3 (RegCM3), but with several improvements, including coupling of Integrated Biosphere Simulator (IBIS) land surface scheme, a new surface albedo assignment method, new convective cloud and convective rainfall autoconversion schemes, and a modified scheme for simulating boundary layer height and boundary layer clouds. To investigate the impact of these more physically realistic representations when incorporated into MRCM, a series of experiments were carried out implementing two land surface schemes [IBIS with a new albedo assignment, and the Biosphere–Atmosphere Transfer Scheme (BATS)] and two convection schemes (Grell with the Fritsch–Chappell closure, and Emanuel in both the default form and modified with the new convective cloud cover and a rainfall autoconversion scheme). The analysis primarily focuses on comparing the rainfall characteristics, surface energy balance, and large-scale circulations against various observations. This work documents significant sensitivity in simulation of the West African monsoon to the choices of the land surface and convection schemes. Despite several deficiencies, the simulation with the combination of IBIS and the modified Emanuel scheme with the new convective cloud cover and a rainfall autoconversion scheme shows the best performance with respect to the spatial distribution of rainfall and the dynamics of the monsoon. The coupling of IBIS leads to representations of the surface energy balance and partitioning that show better agreement with observations compared to BATS. The IBIS simulations also reasonably reproduce the dynamical structures of the West African monsoon circulation.

1. Introduction

Over the past decade, we have worked on improving the skill of the Regional Climate Model, version 3 (RegCM3; Pal et al. 2007), in simulating the climate over different regions through the incorporation of new physical schemes or modification of existing schemes. The version of RegCM3 that includes all of the Massachusetts Institute of Technology (MIT)-based upgrades will be referred to here as the MIT regional climate model (MRCM).

The most significant difference in MRCM relative to the original RegCM3 configuration is coupling with the Integrated Biosphere Simulator (IBIS) land surface scheme (Winter et al. 2009). Based on simulations using IBIS over North America (Winter and Eltahir 2012) and the Maritime Continent (Gianotti et al. 2012), the use of IBIS results in better representation of surface energy and water budgets compared to the Biosphere–Atmosphere Transfer System (BATS) version 1e, which is the default land surface scheme with RegCM3. Furthermore, the addition of a new irrigation scheme to IBIS makes it possible to investigate the effects of anthropogenic land use change over any region (Marcella 2012), while a new surface albedo assignment method used together with IBIS brings further improvement in simulations of surface radiation (Marcella and Eltahir 2012). Another important feature of the MRCM is the recent introduction

────────

Corresponding author address: Dr. Eun-Soon Im, Singapore–MIT Alliance for Research and Technology (SMART) Center for Environmental Sensing and Modeling (CENSAM), 1 CREATE Way, #09-03 CREATE Tower, 138602 Singapore.
E-mail: eunsoon@smart.mit.edu

of new schemes for convective cloud cover and convective rainfall autoconversion (Gianotti 2012; Gianotti and Eltahir 2014a,b). These modifications bring more physical realism into an important component of the model, successfully simulating a convective–radiative feedback, and improving model performance across several radiation fields and rainfall characteristics. Gianotti (2012) and Gianotti and Eltahir (2014a,b) demonstrate that the Emanuel convection scheme incorporating a new convective rainfall autoconversion, used with the new convective cloud scheme, greatly improves the climate simulation over the Maritime Continent compared to the original Emanuel scheme with default cloud cover.

In this study, we evaluate the performance of MRCM in simulating the West African monsoon (WAM) with a focus on the effect of land surface and convection schemes. West Africa is a good test bed to examine the performance of MRCM since previous studies using both global and regional climate models exhibited deficiencies in capturing key characteristics of the WAM (Flaounas et al. 2010; Sylla et al. 2010a,b; Afiesimama et al. 2006; Xue et al. 2010; Hernández-Diaz et al. 2013; Nikulin et al. 2012). Of particular concern is the difficulty in simulating rainfall, because of its strong variability with a wide range of temporal and spatial scales (Gallee et al. 2004; Sylla et al. 2010b). Among several factors that modulate the characteristics of the WAM, the impact of strong land–atmosphere interactions and deep convection will be explored through sensitivity experiments that compare two land surface schemes (IBIS and BATS) and two convection schemes (Grell with the Fritsch–Chappell closure, and Emanuel in both its default form and modified with the new convective autoconversion scheme). These aspects have been chosen for investigation because previous climate modeling studies have shown great sensitivity in model performance to simulation of the land surface and convective processes.

Since West Africa includes a unique transition zone characterized by the sharp gradient between wet and dry climate regimes, it is considered a region of strong coupling between soil moisture and rainfall (Koster et al. 2004). In fact, Steiner et al. (2009) highlighted the role of the land surface scheme and suggested that coupling of the Community Land Model, version 3 (CLM3), can greatly improve simulation of the West African climate within the RegCM3 modeling system. Flaounas et al. (2010) demonstrated using the Weather Research and Forecasting (WRF) model that the convection scheme is critical to simulation of the WAM in terms of the timing of monsoon onset and the rainfall variability.

Several recent studies using various versions of RegCM have reported their efforts to improve the performance of the model in simulating the WAM and to understand the model behavior and sensitivity of the WAM to different model physics (Giorgi et al. 2012; Solmon et al. 2012; Abiodun et al. 2012; Nikulin et al. 2012; Steiner et al. 2009; Sylla et al. 2009, 2010a,b). Although these studies have achieved substantial progress in terms of model improvement and the sensitivity of WAM simulation to model parameters, most of the results still exhibit systematic biases, indicating significant room for improvements in the simulation of key processes. In this study, we build on previous work by providing a comprehensive evaluation of significantly improved physical packages with respect to both land surface and convection schemes. This study will provide a baseline for the performance of MRCM in simulating the WAM. Based on the MRCM control simulation presented in this work, a companion paper (Im et al. 2014) explores the impact of the location, extent, and scheduling of irrigation on simulation of the WAM using the new irrigation scheme of MRCM over the same domain.

2. Model description and experimental design

a. The MIT regional climate model

The MIT regional climate model used in this study is based on the RegCM3 maintained at the International Centre for Theoretical Physics (ICTP) (Pal et al. 2007). The dynamical core of RegCM3 is equivalent to the hydrostatic version of the fifth-generation Pennsylvania State University–National Center for Atmospheric Research (NCAR) Mesoscale Model (MM5; Grell et al. 1994). The physical parameterizations employed in the default RegCM3 configuration include the comprehensive radiative transfer package of the NCAR Community Climate Model, version 3 (CCM3; Kiehl et al. 1996), the nonlocal boundary layer scheme of Holtslag et al. (1990), and the BATS land surface scheme (Dickinson et al. 1993). In the RegCM3 modeling framework, rainfall is derived by the combined process of resolved (grid scale) rainfall as well as unresolved (subgrid scale) rainfall. The resolvable grid-scale rainfall is described using the Subgrid Explicit Moisture Scheme (SUBEX) of Pal et al. (2000). However, several parameters used in SUBEX are different from those of Pal et al. (2000). We used the values recommended at the Fourth ICTP Workshop on the Theory and Use of Regional Climate Models (2008) [e.g., autoconversion rate, $C_{ppt} = 0.25 \times 10^{-3}\,\text{s}^{-1}$; accretion rate, $C_{acc} = 3\,\text{m}^3\,\text{kg}^{-1}\,\text{s}^{-1}$; and raindrop evaporation rate, $C_{evap} = 1.0 \times 10^{-3}\,(\text{kg}\,\text{m}^{-2}\,\text{s}^{-1})^{-1/2}\,\text{s}^{-1}$]. The unresolvable rainfall is produced by a convection scheme, which describes the effects of subgrid-scale convective processes. Among several options for convective parameterization, the Grell scheme (Grell 1993) with the Fritsch–Chappell closure (FC; Fritsch and Chappell

TABLE 1. Summary of MRCM upgrade features and key references.

Upgrade features	References
Coupling of IBIS land surface scheme	Winter et al. (2009)
New surface albedo assignment	Marcella (2012), Marcella and Eltahir (2012)
New convective cloud scheme	Gianotti (2012), Gianotti and Eltahir (2014a)
New convective rainfall autoconversion scheme	Gianotti (2012), Gianotti and Eltahir (2014b)
Modified boundary layer height and boundary layer cloud scheme	Gianotti (2012)

1980) and Emanuel scheme (Emanuel and Zivkovic-Rothman 1999) are the most popular in the RegCM user group. Previous work applying RegCM3 to different target regions indicates that the Grell (Emanuel) scheme generally tends to underestimate (overestimate) the rainfall.

The major upgrade features included in the MRCM are summarized in Table 1. The most important change contained within MRCM compared to the default RegCM3 configuration is coupling with the land surface scheme IBIS (Winter et al. 2009). IBIS is a dynamic global vegetation model that uses a modular, physically consistent framework to perform integrated simulations of water, energy, and carbon fluxes. IBIS possesses several key advantages over BATS, most notably vegetation dynamics, the coexistence of multiple plant function types within the same grid cell, sophisticated plant phenology, plant competitions, explicit modeling of soil and plant biogeochemistry, and additional soil and snow layers [see Winter et al. (2009) for a more detailed description]. In addition to coupling with IBIS, the surface albedo over the deserts of northern Africa and southwest Asia is adjusted within MRCM using a statistical correction (Marcella and Eltahir 2012).

MRCM also includes improvements that show more realistic representations of boundary layer processes, convective cloud cover and convective rainfall production. Modifications were made to the representation of the planetary boundary layer (PBL) height to reduce an erroneously high nocturnal PBL height, resulting in a simulated PBL height that matches closely to observations over Singapore (Gianotti 2012). Modifications were also made to the representation of nonconvective cloud cover within the PBL by introducing a bulk relative humidity threshold over the mixed layer, which removed unrealistic low-level cloud cover over land and provided a better match between simulated cloud cover and observations from the International Satellite Cloud Climatology Project (ISCCP) (Gianotti 2012).

A new method for representing the horizontal factional coverage of convective cloud is introduced, which utilizes a relationship between the simulated amount of convective cloud water and typical observations of convective cloud water density. This method allows for simulation of a realistic convective–radiative feedback that was absent in the previous version of the model and is completely independent of model resolution (Gianotti and Eltahir 2014a). Finally, a new method for parameterizing convective autoconversion (the conversion of convective cloud liquid water into rainfall) is included with MRCM, which is derived from observed distributions of cloud water content and is constrained by observations of cloud droplet characteristics and climatological rainfall intensity. This method, combined with the other upgrades to simulated convective cloud cover and PBL processes, results in significant improvements to the simulation of convective rainfall, surface shortwave radiation, net radiation, and turbulent heat fluxes (Gianotti and Eltahir 2014b).

b. Experimental design

Figure 1 shows the model domain and land-use distribution used for simulations with BATS and IBIS land surface schemes. The domain covers the western region of Africa and portions of the Atlantic Ocean extending in the south and west directions (10°S–38°N and 32°W–27°E, including the buffer area). It is centered at 15°N, 3°W with 50-km resolution. The three subregions outlined in Fig. 1b are used for an area-averaged analysis. IBIS is used here assuming static vegetation conditions. While the vegetation biomes for the IBIS simulations are assigned using the potential global vegetation dataset of Ramankutty and Foley (1999), BATS uses the Global Land Cover Characterization (GLCC) dataset for the vegetation/land cover type. This results in some differences in prescribed vegetation, primarily around the Guinean coast: the BATS land cover is primarily a mix of tall grass and forest/field mosaic, which the IBIS land cover comprises tropical evergreen and savanna.

Table 2 summarizes the varying characteristics of the simulation experiments presented in this study. As mentioned in the introduction, two land surface schemes, IBIS and BATS, are used with the abbreviations I and B in the experiment title, while two convection schemes, Grell with the Fritsch–Chappell closure and Emanuel are used with the abbreviations GF and E. The standard Emanuel scheme (i.e., with all default settings) is denoted by SE, while the modified version, which contains the new autoconversion method used in conjunction with all other model upgrades described above, is denoted by ME. In addition to the physics parameterizations, we also examine the impact of the initial and

(a) BATS land-use   (b) IBIS land-use
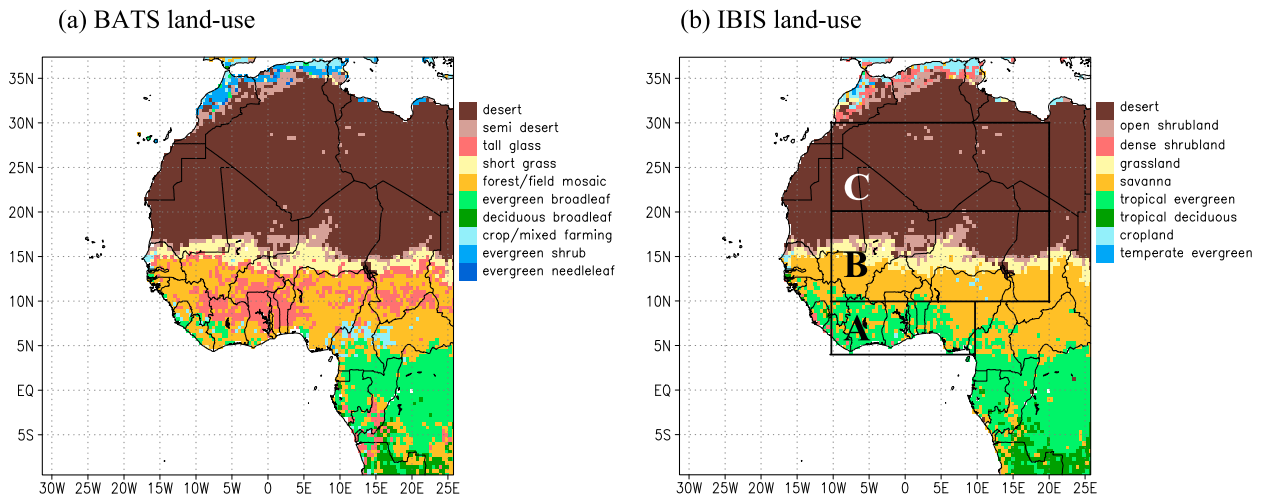

FIG. 1. Model domain and land-use distribution used for (a) BATS and (b) IBIS simulations. The three subregions (A: Guinean coast, B: Sahel, and C: northern Africa) for area-averaged analysis are outlined in (b).

boundary conditions. In most simulations, the initial and lateral boundary conditions are obtained from the European Centre for Medium-Range Weather Forecasts (ECMWF) Interim Re-Analysis (ERA-Interim) with a resolution of $1.5° \times 1.5°$ (Uppala et al. 2008). However, for a comparison, one simulation is driven by the 40-yr ECMWF Re-Analysis (ERA-40) with a resolution of $2.5° \times 2.5°$ (Uppala et al. 2005). Both lateral boundary conditions are prescribed to the regional climate model every 6 h (four times a day). Uppala et al. (2008) documents that the ERA-Interim corrects the errors in the hydrologic cycle variables embedded in ERA-40, thus it is expected that the ERA-Interim provides more accurate large-scale forcing compared to ERA-40. For the sea surface temperature (SST) over the oceanic areas, the National Oceanic and Atmospheric Administration (NOAA) optimum interpolation (OI) SST dataset with a horizontal resolution of $1° \times 1°$ is used at a weekly resolution. For the purpose of specifying the initial conditions for IBIS, an offline version of IBIS was forced by prescribed atmospheric data, and the resulting equilibrium conditions (soil moisture and soil temperature for each soil layer) were used for the initialization of soil conditions. The simulations using ERA-Interim span a period of 20 yr from January 1989 to December 2008,

whereas the simulation using ERA-40 spans a period of 13 yr from January 1989 to December 2001. All simulations are continuously integrated throughout whole period, and additional spinup time is not assigned. However, this should not introduce a significant problem because our analysis is focused on the summer season. Therefore, the four 20-yr simulations and one 13-yr simulation are compared to investigate the impact of land surface and convection schemes and boundary conditions. For example, the two simulations BSEIN and ISEIN are identical aside from the choice of land surface scheme. Therefore, their comparison gives insight into the difference between the BATS and IBIS schemes.

Simulations are evaluated against both observations and reanalysis data. To assess the performance of the model in simulating rainfall, the Climate Research Unit (CRU) time series 2.0 (TS2.0) (Mitchell et al. 2004) and the Global Precipitation Climatology Project (GPCP) monthly precipitation dataset (Adler et al. 2003) are used. CRU has a horizontal resolution of $0.5° \times 0.5°$ over only land area, while GPCP has $2.5° \times 2.5°$ global coverage. The outgoing longwave radiation (OLR) data with a resolution of $2.5° \times 2.5°$ are also used for validation. The OLR data are estimated from NOAA polar-orbiting satellites, and missing values because of

TABLE 2. Summary of simulation characteristics.

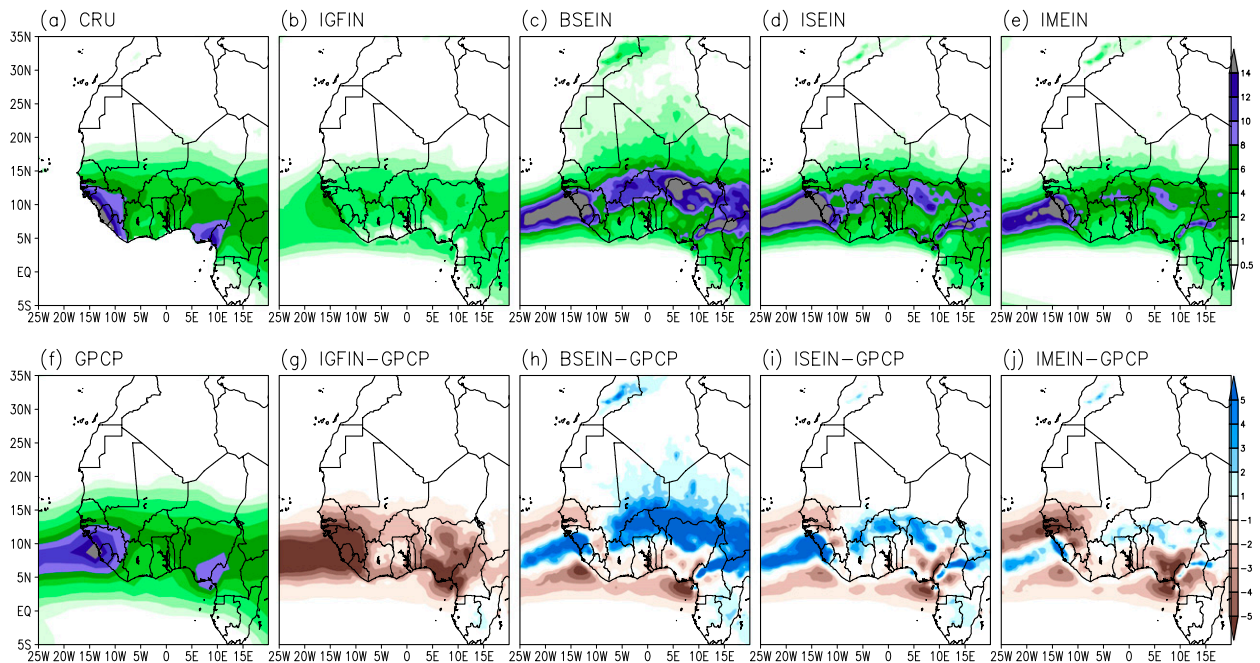| Simulation name	Land surface scheme	Convection scheme	Initial and boundary condition (period)
IGFIN	IBIS	Grell FC	ERA-Interim (1989–2008; 20 yr)
BSE40	BATS	Standard Emanuel	ERA-40 (1989–2001; 13 yr)
BSEIN	BATS	Standard Emanuel	ERA-Interim (1989–2008; 20 yr)
ISEIN	IBIS	Standard Emanuel	ERA-Interim (1989–2008; 20 yr)
IMEIN	IBIS	Modified Emanuel	ERA-Interim (1989–2008; 20 yr)

FIG. 2. Spatial distribution of mean northern summer (JJA) precipitation (mm day^{-1}) from the (a) CRU and (f) GPCP observations, (b)–(e) four experiments, and (g)–(j) their differences with GPCP observations.

incomplete global coverage are interpolated by the algorithm described in Liebmann and Smith (1996). The simulated surface energy budget components are evaluated against the National Aeronautics and Space Administration (NASA) Surface Radiation Budget (SRB) version 3.0 dataset during 1989–98 (Gupta et al. 1999). The simulated latent and sensible heat fluxes, vertical wind fields, and pressure velocity are compared to ERA-Interim. Even though reanalysis products do not constitute direct observations, they present a feasible alternative way for assessing the model performance over this region, given the scarce observational coverage.

3. Results

a. Rainfall

We begin our analysis of the climatological aspects of rainfall during the northern summer season. Figure 2 presents the spatial distribution of June–August (JJA) mean rainfall derived from CRU and GPCP observation, the four experiments with the 20-yr period, and their differences with GPCP observations. During JJA, the spatial distributions of simulated rainfall exhibit a meridional gradient with rainfall decreasing in intensity from the southern Sahel to northern Africa in association with the latitudinal migration of the intertropical convergence zone (ITCZ). The localized maxima offshore from the western coast of Guinea along 5°–10°N,

over the Fouta-Jalon, over the Cameroon mountains, and over the Soudano-Sahelian region including northern Nigeria are features common to all the simulations.

Although all simulations exhibit different results in terms of rainfall amount and localization, they can be divided into three general categories of bias: too dry, too wet, and a moderate mixed pattern. The IGFIN simulation with the Grell FC convection scheme excessively underestimates the rainfall, showing a strong dry bias throughout the entire Guinean coast and the southern Sahel. Using the Emanuel convection scheme, the BSEIN simulation with the BATS land surface scheme shows an excessive wet bias across the Sahel and unrealistic rainfall north of 18°N, while ISEIN and IMEIN with the IBIS land surface scheme show a mixed bias pattern of relatively moderate magnitude compared to the other simulations.

The common deficiency in all simulations appears in the southwestern coast of the Guinean region and the coastal region near the Cameroon mountains. All models fail to accurately capture the intensity of the localized maximum over those regions regardless of the convection or land surface scheme, thereby showing a significant dry bias. Such a systematic bias is not limited to our simulations, but rather seems to be a typical error found in many other regional climate simulations over West Africa (Flaounas et al. 2010; Sylla et al. 2009, 2010a,b; Hernández-Diaz et al. 2013; Zaroug et al. 2013).

When comparing the two land surface schemes, the IBIS simulations (ISEIN and IMEIN) are quantitatively in better agreement with the observed estimates, presenting a substantial reduction in the wet biases produced by BSEIN. In addition, the IMEIN simulation with modified Emanuel scheme tends to simulate less rainfall. This improves the wet bias over the southern Sahel, but it worsens the dry bias over the southwestern coast of the Guinean region and the coastal area near the Cameroon mountains.

Because of the relatively short integration period of the BSE40 simulation, we exclude it from Fig. 2. Comparing BSE40 and BSEIN during the 13-yr period 1989–2001, the spatial correlation of JJA mean rainfall is 0.98, indicating that both simulations are mostly similar. In case of area-averaged values of JJA mean rainfall over land, BSE40 and BSEIN are 4.3 and 4.1 mm day^{-1}, which are much higher than observed value (CRU is 2.6 mm day^{-1} and GPCP is 2.6 mm day^{-1}). Overall, the BSE40 simulation tends to make the wet bias worse compared to BSEIN, but their general behaviors are very similar (not shown). Therefore, we conclude that the effect of initial and lateral boundary condition (ERA-40 versus ERA-Interim) seems to be less significant, compared to the land surface and convection schemes. To facilitate the comparison, the four simulations with the same period of 20 yr are presented in the following analysis.

To provide a more quantitative measure of model performance, rainfall seasonal cycle is presented in Fig. 3 for rainfall averaged over the three regions (the Guinean coast, Sahel, and northern Africa) displayed in Fig. 1. The four simulation results and CRU observation based on the 20-yr climatology are presented in this figure. The seasonality of the monthly mean rainfall shows a regional dependency, highlighting the pronounced spatial complexity of the monsoon rainfall over West Africa. From CRU estimates over the Guinean coast, the temporal evolution of rainfall exhibits a slight bimodal structure, having two peaks in June and September. The IMEIN simulation demonstrates the most capability out of the four experiments in capturing the timing of these rainfall peaks despite some underestimation, showing good phase coherence with the observed variation. The BSEIN simulation also exhibits a bimodal distribution; however, they display errors in not only quantitative overestimation (except for July and August) but also the timing of peak occurrence. These simulations produce the first peak too early (May) and second peak too late (October) with overestimation of both peaks, whereas they underestimate the rainfall intensity during the northward migration of the West African monsoon to the Sahel region (over July and August).
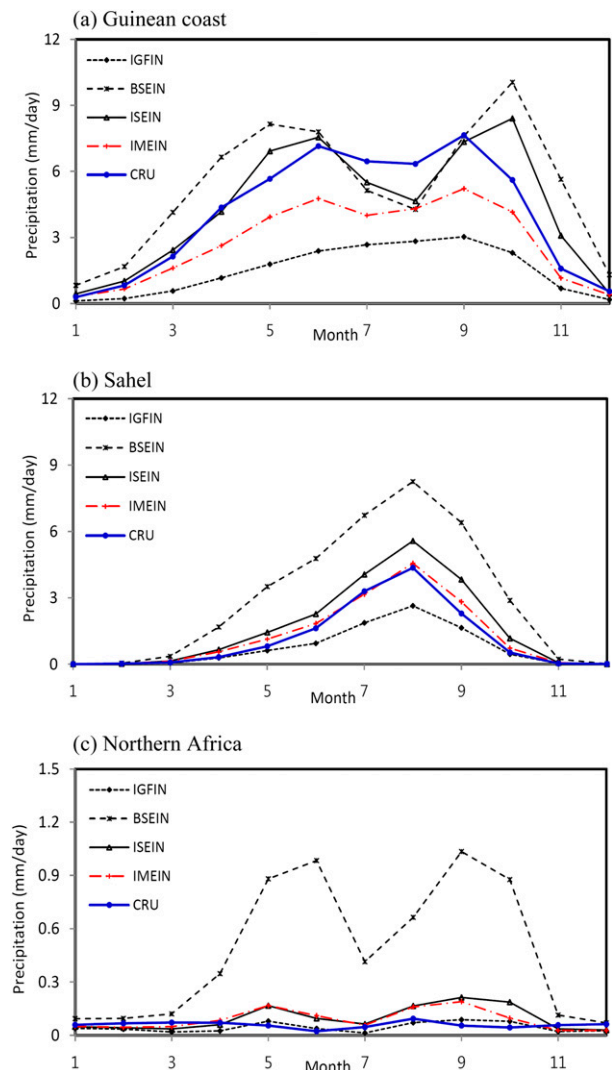

FIG. 3. Monthly mean variation of area-averaged precipitation over the (a) Guinean coast, (b) Sahel, and (c) northern Africa subregions from the four experiments and CRU observation during 20 yr (1989–2008).

This error is a clear indication of inaccurate simulation of the propagation of the monsoon rainfall northward.

For the Sahel region, all simulations reproduce the observed peak timing in August; however, the corresponding intensities are considerably different across the simulations. The IMEIN simulation shows the best performance, being much closer to the observations than the other simulations and almost exactly matching the observed peak (IMEIN is 4.6 mm day^{-1} and CRU is 4.4 mm day^{-1}). On the other hand, the BSEIN simulation overestimates the peak intensity up to approximately 2 times (189%). The overestimation errors of both BATS simulations are even more exaggerated in northern Africa. The BATS land surface scheme tends
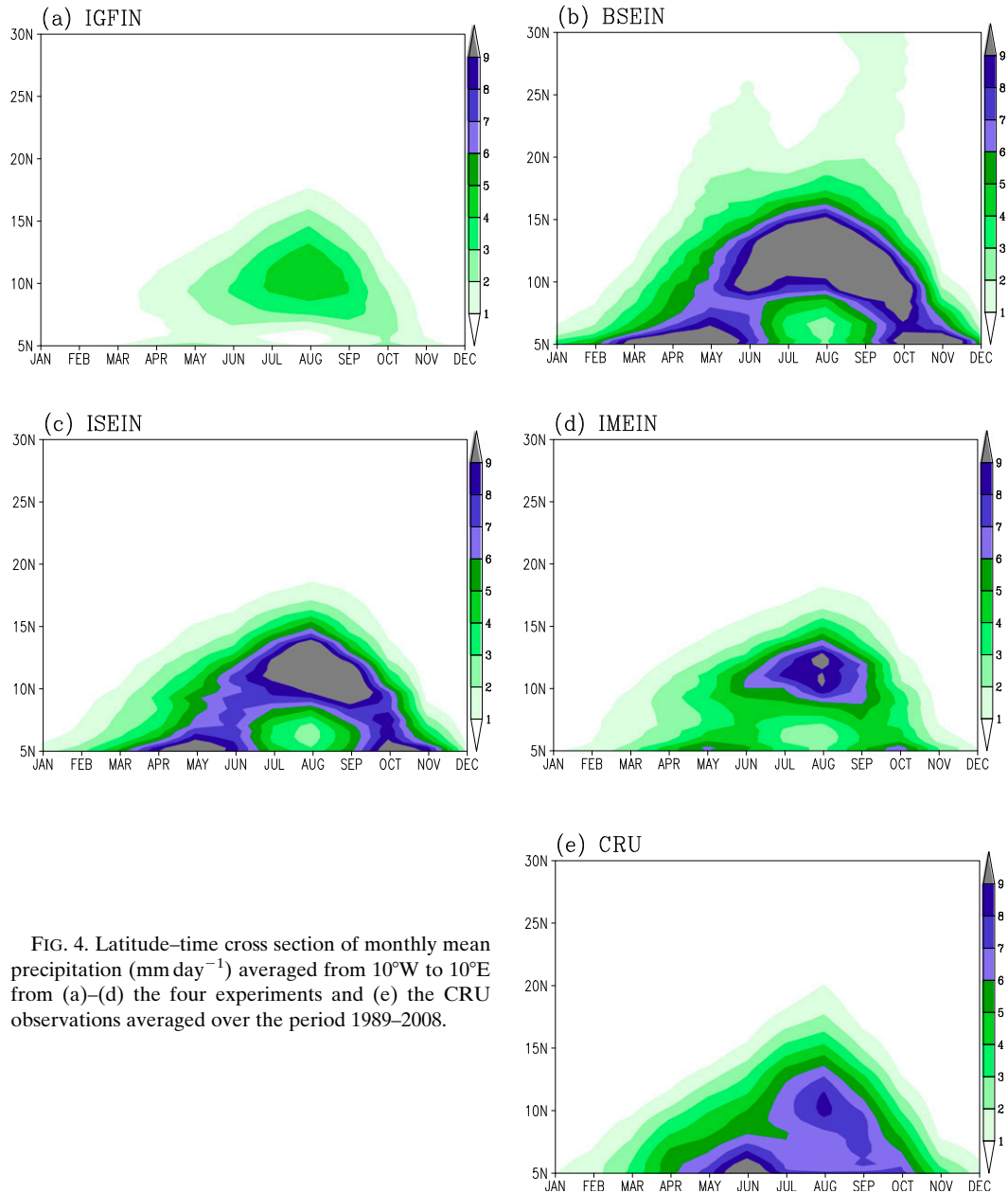
FIG. 4. Latitude–time cross section of monthly mean precipitation (mm day^{-1}) averaged from 10°W to 10°E from (a)–(d) the four experiments and (e) the CRU observations averaged over the period 1989–2008.

to produce unrealistic rainfall over very dry desert regions, again exposing the model deficiency in overestimating the rainfall as seen in Figs. 2c and 2h.

One important feature of the WAM is the northward propagation and gradual retreat of the rainfall (Le Barbé et al. 2002; Sultan and Janicot 2000; Sylla et al. 2010b; Nikulin et al. 2012; Hernández-Diaz et al. 2013). Figure 4 shows the latitude–time cross section of the zonally averaged monthly rainfall over the period 1989–2008 along 10°W–10°E for the CRU observations and the simulations using the ERA-Interim boundary conditions. The seasonal advance and retreat of the summer

monsoon behaves in a stepwise rather than a continuous manner, indicated by northward jumps of maximum rainfall. Both the simulations and observations display abrupt phase transitions for the onset, maximum, and retreat of the monsoon rainfall, with differing magnitudes (Eltahir and Gong 1996; Sultan and Janicot 2000). For the CRU distribution, it is observed that the first major quasi-stationary monsoon front appears near 5°N in May, which corresponds to the onset of the monsoon along the Guinean coast. Then the high-intensity rainband jumps toward the Sahel region and the maximum appears around 9°–12°N in August. The rainfall amount
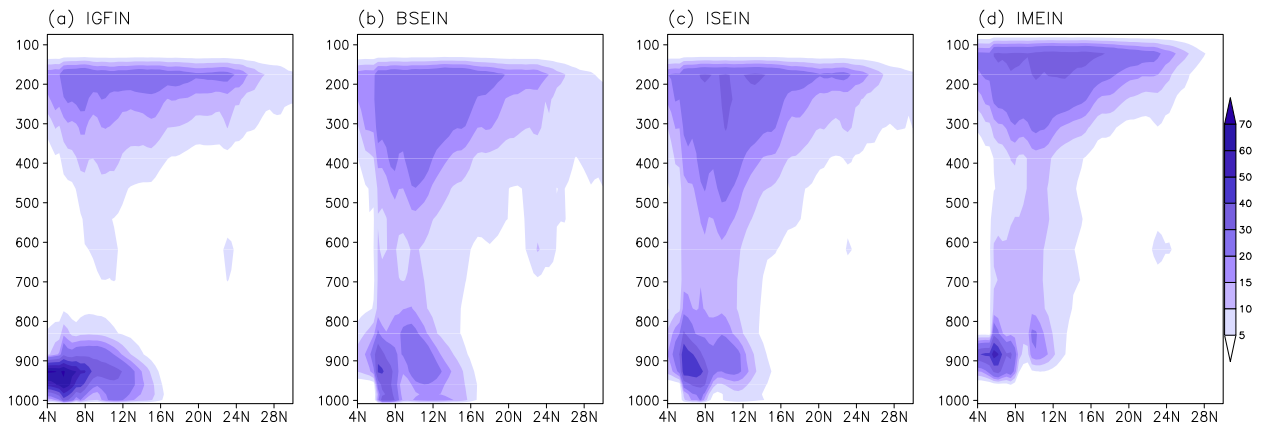
FIG. 5. Vertical cross section of cloud fraction for the summer season (JJA) at 5°E from the four experiments averaged for the period 1989–2008. The vertical axis shows pressure in hectopascals (hPa). (Unit is fractional horizontal coverage of grid cell.)

during August, when the monsoon generally reaches its peak, is less than that of the onset period in May. The high amounts of rainfall, of more than 6 mm day^{-1}, end around October after the monsoon retreat toward the Guinean coast.

All simulations reproduce the maximum in the Sahel region occurring in August, with different magnitudes. However, all simulations tend to underestimate the rainfall amount along the Guinean coast during that period, which is probably due to a jump of maximum rainfall farther north than observed. The IGFIN simulation tends to underestimate the rainfall amounts during both onset and maximum period of WAM, while the BSEIN and ISEIN simulations tend to overestimate them. The results are consistent with previous studies showing that the Grell convection scheme tends to underestimate rainfall and the Emanuel scheme tends to overestimate it. However, the rainfall amount in IMEIN agrees reasonably well with observations during August with some small overestimation, although it underestimates the rainfall intensity along the Guinean coast during May and around 5°–10°N during June and September, consistent with the results found in the spatial and temporal pattern of rainfall in Figs. 2 and 3. One weakness of all the simulations is a failure to capture the asymmetric behavior of the rainfall amount between the onset and retreat periods as seen in the CRU pattern. The BSEIN and ISEIN simulations produce much longer and stronger retreat phases compared to observations. In addition to the superiority of IMEIN over other simulations in terms of extent and intensity of maximum rainfall around August, its performance is also comparable to simulations in the Coordinated Regional Downscaling Experiment in Africa (CORDEX-Africa) reported by Nikulin et al. 2012 (see Fig. 8).

Overall, Figs. 2–4 indicate significant sensitivity in simulations of the WAM to the choices of land surface and convection schemes. In particular, the improvement in simulation of the spatial distribution and seasonal variation of rainfall evident in the simulations with the IBIS land surface scheme is comparable with the improvement shown in Steiner et al. (2009) using RegCM3 coupled with CLM3. Steiner et al. (2009) demonstrate that the coupling with CLM3 could substantially improve simulation of the WAM with RegCM3 relative to coupling with the BATS scheme, reducing strong wet bias. The work presented here supports the assertion that parameterizations of the land surface are critical for improving model performance for the WAM.

In spite of applying the same land surface and convection schemes, ISEIN and IMEIN show fairly different results, indicating that the modifications made to cloud cover and autoconversion are the main driver of the different behavior between these simulations. Generally, it has been shown in earlier studies that the Emanuel scheme tends to produce higher rainfall amounts than the Grell scheme over tropical regions within the RegCM3 modeling system (Pal et al. 2007; Steiner et al. 2009). Since the modifications incorporated in IMEIN tends to reduce the simulated rainfall amount, IMEIN shows improvement with respect to the preexisting strong wet bias in ISEIN but worsens the dry bias.

b. Clouds

Figure 5 presents the vertical cross section of cloud fraction (i.e., fractional horizontal coverage of grid cell) at 5°E for the four simulations using the ERA-Interim boundary conditions, averaged over the JJA season for the period 1989–2008. We present the cross section at 5°E because this location exhibits significant differences among the simulations and corresponds to the longitude

of localized maximum rainfall. The simulated cloud profiles exhibit differences that reflect the various influences of the convection scheme and modifications made within MRCM. The choice of land surface scheme appears to have a relatively small impact on the simulated cloud cover.

The IGFIN simulation exhibits more extensive cloud cover in the lowest 100 hPa of the atmosphere than the other simulations, but less cloud cover throughout the rest of the vertical column. This reflects the weaker convective activity simulated by the Grell scheme compared to the Emanuel scheme: the Grell scheme generates less vertical transport due to convective mass flux, such that moisture generated at the surface resulting from latent heat flux largely remains in the lower atmosphere. This build-up of moisture is then converted into large-scale cloud cover by the SUBEX scheme within RegCM3. The weak vertical transport simulated by the Grell scheme results in little high cloud cover owing to the comparatively small volume of moisture transported aloft.

In contrast, the simulations using the Emanuel scheme show less low-level cloud cover but more extensive cloud cover throughout the vertical column and especially at high altitudes. This results from the strong convective mass flux generated by this convection scheme, which transports large volumes of moisture vertically through the atmosphere and produces large anvil clouds aloft. The differences between BSEIN and ISEIN are relatively small compared to the differences between IGFIN and these two Emanuel simulations, indicating that the turbulent heat fluxes generated by the different land surface schemes play a less significant role in cloud formation than the strength of the convective mass flux.

The IMEIN simulation exhibits a cloud profile that appears shifted vertically compared to the other simulations, with very little cloud cover in the lowest 100 hPa of the atmosphere and more cloud cover within the top 100 hPa of the vertical column. These differences are associated with modifications made by Gianotti (2012). The representation of large-scale cloud cover within the PBL was modified such that cloud could only form within the mixed PBL if its entire depth was saturated. This was found to remove unrealistic dense cloud cover close to the surface over land and improve the model performance compared to the ISCCP observations (Gianotti 2012). Figure 5 illustrates that this modification had a similar impact over West Africa as was documented over the Maritime Continent, inhibiting the formation of extensive low-level cloud cover. A second modification made in Gianotti (2012) was to increase the altitude at which cloud was permitted to form within RegCM3, extending the allowable cloud top to

approximately 17-km elevation (compared to the default setting of about 14 km). Since the tropical troposphere is observed to extend to nearly 18 km, Fig. 5 indicates that the default version of RegCM3 unrealistically limited the vertical extent of simulated cloud cover, which is rectified in IMEIN.

The time-mean cloud profile in IMEIN does not appear substantially different from BSEIN or ISEIN aside from being vertically shifted, as already mentioned. However, it was found that the temporal evolution of the cloud profile is substantially different between these simulations (not shown). In particular, the diurnal cycle of cloud cover is shifted from a nighttime peak in BSEIN and ISEIN to an early afternoon peak in IMEIN. This is the result of two major changes contained within IMEIN—new parameterizations for convective cloud cover and autoconversion of convective rainfall. Although these changes are not evident in Fig. 5, they have significant impacts on the simulation of incoming solar radiation and rainfall production, as described in sections 3a and 3c.

As another indicator to represent the effect of changes in convection scheme on clouds, we compare the spatial distribution of OLR. It is known that OLR is characteristic of convective activity and the resultant cloudiness (Fontaine et al. 2008). Low values of OLR correspond to the presence of high cloudiness because the clouds tend to emit radiation upward, from relatively cold altitudes. Figure 6 presents the spatial distribution of JJA mean OLR from NOAA estimates and the four simulations. To clearly identify the anomalies in OLR of individual simulation from observed pattern, we also present the differences between four simulations and NOAA observations. All simulations generally reproduce the broad patterns observed, such as high values over northern Africa and a minimum band along the Guinean coast and southern Sahel. However, quantitative discrepancies with observations reflect their different performances, which seem to be associated with differences in rainfall and clouds simulations. For example, BSEIN characterized by excessive wet bias of rainfall shows a predominant negative bias across entire land area. On the contrary, IGFIN shows a positive bias in the western coast of Guinea where a strong dry bias is simulated. Compared to other simulations, IMEIN shows relatively less bias of OLR. In this regard, it is reasonable to conclude that the new clouds and rainfall formation schemes introduced by Gianotti (2012) and Gianotti and Eltahir (2014a,b) bring some improvements in simulations of convection and cloudiness.

c. Surface energy balance

In addition to the significant differences in simulated rainfall and cloud cover characteristics presented in
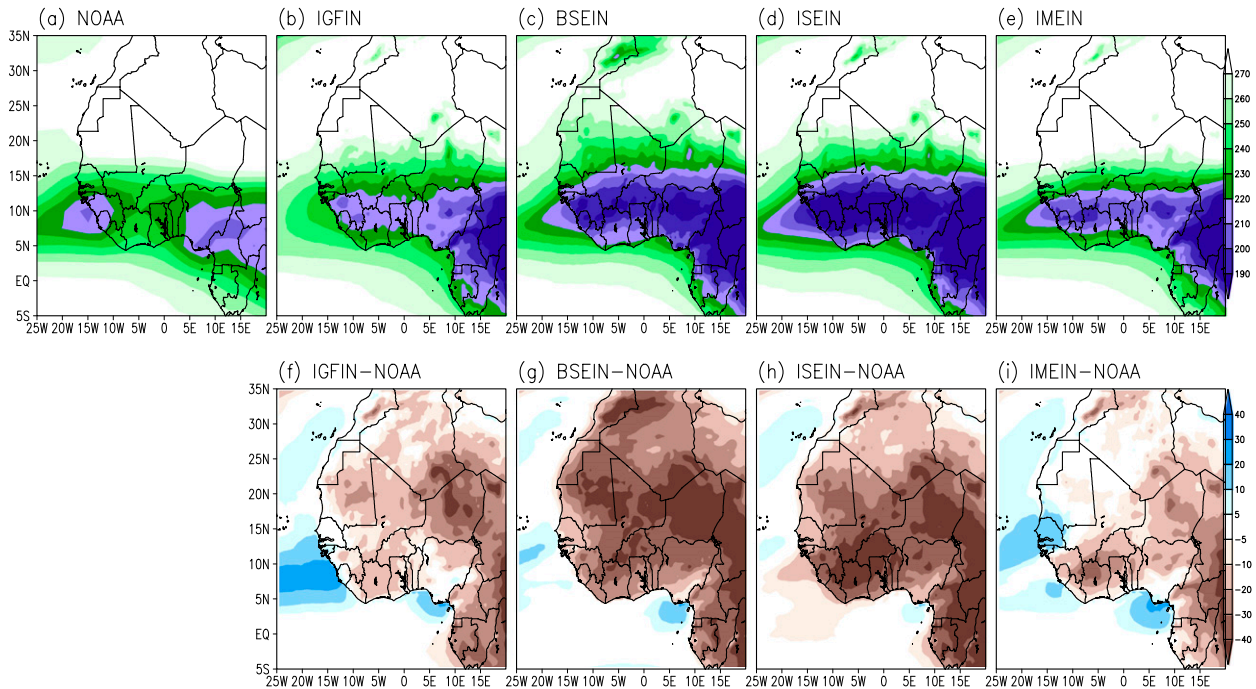
FIG. 6. Spatial distribution of JJA mean top of the atmosphere OLR (W m^{-2}) from (a) the NOAA observation and (b)–(e) the four experiments, and (f)–(i) their differences.

sections 3a and 3b, it is expected that the implementation of different land surface and convection schemes would also lead to differences in the simulated surface energy distribution and partitioning. Table 3 provides the major components of the surface energy budget, including both radiative and turbulent heat fluxes, averaged over the three analysis regions (Guinean coast, Sahel, and northern Africa) during the summer season (JJA) for the period of 1989–98. Beside our simulations, we also provide the results from Steiner et al. (2009) (using BATS labeled S_BATS, and CLM3 labeled S_CLM in Table 3). Note that absolute comparisons between our simulations and those of Steiner et al. (2009) are necessarily limited in scope because our integration periods, initial and boundary conditions, and analysis regions over the Sahel and northern Africa are not exactly the same. Therefore, the intent of this comparison is to investigate roughly the different behaviors produced by different land surface and convection schemes, in particular focusing on our IBIS simulations and CLM3 simulations from Steiner et al. (2009). We choose to focus on the Steiner et al. (2009) results because these represent the state of the art describing the skill of RegCM3 in simulating the WAM.

The incoming surface solar radiation is an important variable characterizing the conditions at the land–atmosphere interface. While the IMEIN simulation matches the observations well for the Guinean coast, it tends to significantly overestimate this variable over

the Sahel and northern Africa. This overestimation can be at least partially explained by the lack of representation of mineral aerosols in all the simulations. Simulations of incoming solar radiation in the other simulations (IGFIN, BSEIN, and ISEIN) reflect to a significant degree their respective errors in simulating clouds and rainfall.

Table 3 shows that the simulated net radiation, which describes the balance between incoming and outgoing radiation fluxes at the surface, is significantly different across our simulations. Compared to the excessive net radiation of the BATS simulation (BSEIN), the IBIS simulations are quantitatively in better agreement with observations. It is important to note that the net radiations simulated by S_BATS and S_CLM are similar between the Guinean coast and northern Africa, lacking the latitudinal gradient decreasing in magnitude from south to north as shown in the observations. Thus, both simulations tend to agree with observations over the Guinean coast while significantly overestimating net radiation over the Sahel and northern Africa, with error of 100% in the latter case. This implies that even though the S_CLM simulation shows improvement in simulated rainfall and temperature compared with the S_BATS simulation (see Figs. 3 and 12 in Steiner et al. 2009), such improvements are not a result of the corresponding improvements in the surface radiation budget. In fact, larger errors occur in the S_CLM simulation with respect to both incident and absorbed shortwave

TABLE 3. Surface energy balance components (W m^{-2}) derived from the four experiments, observations (OBS, radiative fluxes from SRB data and heat fluxes from ERA-Interim), and Steiner et al. (2009; S_BATS and S_CLM). Shown are the components for incoming shortwave (SW In), absorbed shortwave (SW Abs), net longwave (Net LW), net radiation (Net R), sensible heat flux (SH), latent heat flux (LH), and ground heat flux (GH).

		IGFIN	BSEIN	ISEIN	IMEIN	OBS	S_BATS	S_CLM
Guinean coast	SW In	170.7	203.9	185.5	184.8	183.5	170.9	197.5
	SW Abs	142.7	179.6	157.0	154.8	150.1	147.6	153.7
	Net LW	30.2	31.2	29.3	36.2	32.9	33.8	36.1
	Net R	112.5	148.4	127.7	118.5	117.2	113.8	117.6
	Albedo	0.16	0.12	0.15	0.16	0.18	0.14	0.22
	SH	43.5	21.4	14.9	23.2	16.6	9.0	4.9
	LH	65.5	109.4	98.5	86.8	94.3	110.6	79.3
	GH	5.1	17.7	16.6	10.6	6.3	−5.8	33.4
Sahel	SW In	272.2	256.5	261.5	278.9	262.1	236.3	288.3
	SW Abs	191.3	204.1	185.3	196.8	180.4	187.3	214.3
	Net LW	85.7	62.6	79.2	85.7	83.4	59.4	82.6
	Net R	105.5	141.5	106.1	111.1	97.0	127.9	131.7
	Albedo	0.30	0.20	0.29	0.29	0.31	0.21	0.26
	SH	65.1	57.1	47.7	60.1	53.7	40.30	44.10
	LH	42.0	86.5	59.6	52.0	55.2	98.30	62.90
	GH	−0.6	−2.2	0.2	0.1	−11.9	−10.7	24.7
Northern Africa	SW In	348.3	329.4	339.8	352.1	303.4	319.6	344.6
	SW Abs	225.9	239.8	221.9	229.8	212.2	232.7	249.9
	Net LW	158.4	130.5	153.1	150.9	154.5	116.6	135.1
	Net R	67.5	109.3	68.7	78.9	57.7	116.1	114.8
	Albedo	0.35	0.27	0.35	0.35	0.30	0.27	0.27
	SH	62.8	92.9	61.4	73.9	71.6	92.4	86.9
	LH	1.7	16.1	4.3	3.9	3.2	25.3	10.5
	GH	3.1	0.3	3.2	1.2	−17.1	−1.6	17.4

radiation at the surface compared to the SRB observations. Therefore it appears that surface radiation biases simulated by the BATS land surface scheme are not adequately addressed by the CLM3 land surface scheme.

Figure 7 shows the monthly mean meridional distributions of net radiation, zonally averaged over 10°W–10°E from the four experiments and the SRB observations. The impact of the land surface scheme on the model performance is clearly illustrated in this figure, with net radiation responding more sensitively to the choice of land surface scheme than convection scheme. Figure 7 also indicates that a much more realistic representation of net radiation is simulated by IBIS than by BATS with reasonable performance in capturing the seasonal variation and latitudinal distribution of net radiation, which is consistent with the area-averaged values shown in Table 3. Compared to SRB, the BSEIN simulation tends to systematically overestimate net radiation. In particular, BSEIN exhibits a bias in net radiation over northern Africa of about 60 W m^{-2} during the summer season. This excess surface energy contributes to an environment that is favorable for convection, as evident in the unrealistic rainfall simulated over northern Africa (Fig. 4b).

One reason for the simulation of too much net radiation in BSEIN is underestimation of the surface albedo. Figure 8 shows the spatial distribution of surface albedo for the summer season (JJA) derived from the four experiments and the SRB observations. This figure suggests a problem embedded in the BSEIN simulation, where surface albedo is consistently lower over land than the SRB observations and lacking the appropriate spatial variation. Since the surface albedo determines the ratio of solar radiation reflected by the surface to incident solar radiation, a lower albedo results in more absorbed solar radiation. Steiner et al. (2009) also noted that the surface albedo was too low in their simulation using BATS, and attributed this result to higher soil moisture. Since wetter soils further reduce the soil albedo, this can cause an enhanced feedback to absorbed solar radiation, leading to excessive net radiation. Figure 8 shows that the surface albedo is satisfactorily simulated in the IBIS simulations. The spatial variations reasonably represented when compared with observed patterns, with values agreeing better with observations except north of 15°N where the simulated albedo is overestimated. It is worth noting that the bias of albedo is more a reflection of prescribed input data for surface properties such as soil color and soil texture rather than
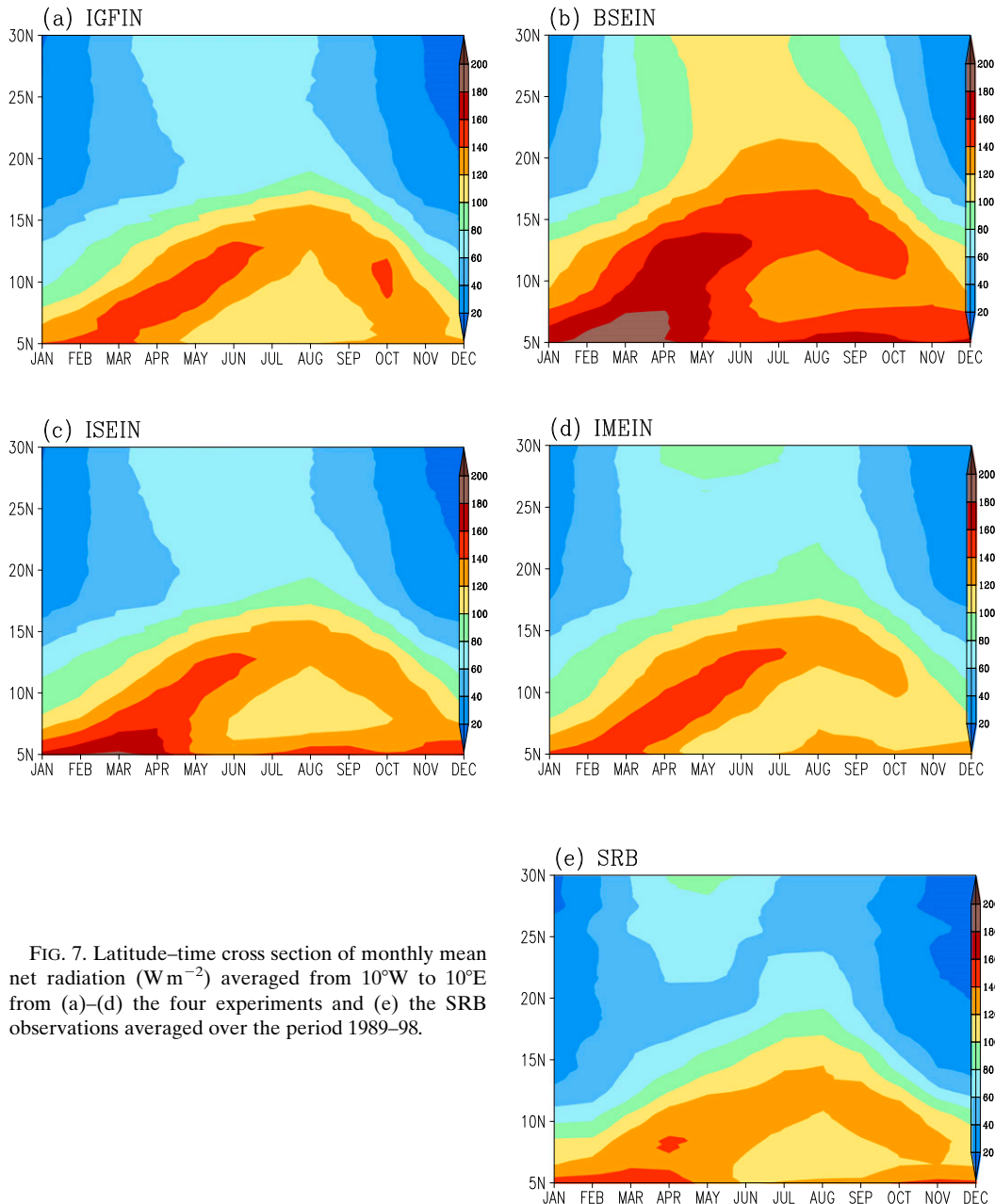
FIG. 7. Latitude–time cross section of monthly mean net radiation (W m^{-2}) averaged from 10°W to 10°E from (a)–(d) the four experiments and (e) the SRB observations averaged over the period 1989–98.

an intrinsic feature of the model itself. Different land surface models have their own way to quantify the impact of vegetation and soil moisture on albedo. In this regard, strongly underestimated albedo of BSEIN over the desert region is largely caused by the uncertainty of soil color or dry soil properties prescribed by BATS land surface scheme.

Considering the simulation of the surface turbulent heat fluxes, Table 3 indicates that latent and sensible heat fluxes show significant sensitivity to the choice of

land surface and convection schemes. Total surface heat flux is defined as the sum of the latent, sensible, and ground (soil) heat fluxes, and it is balanced by the surface net radiation. However, since the ground heat flux should be negligible over long time scales (since the land does not accumulate heat), the surface energy budget is strongly influenced by the relative partitioning of latent and sensible heat fluxes. Note that the observed ground heat flux given in Table 3 includes some uncertainty because it is not based on actual measurements, but
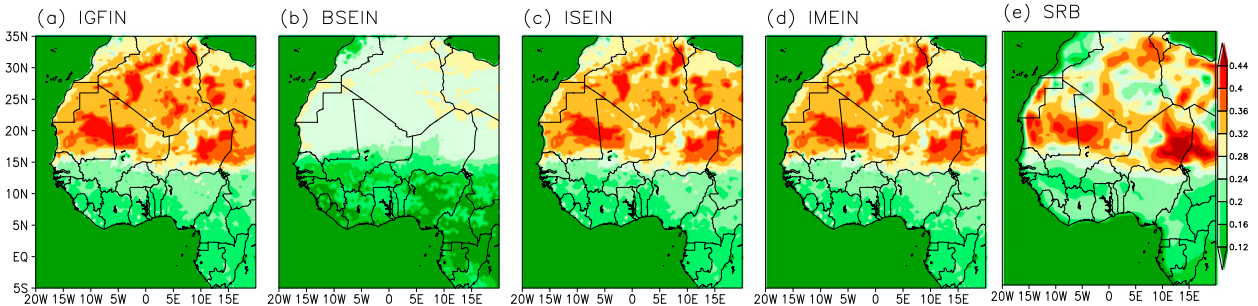
FIG. 8. Spatial distribution of surface albedo for the summer season (JJA) from (a)–(d) the four experiments and (e) the SRB observations averaged over the period 1989–98.

rather is derived from the difference between the net radiation from the SRB observations and the latent and sensible heat fluxes of ERA-Interim.

The observed latent and sensible heat fluxes show opposing latitudinal gradients, respectively decreasing northward and southward pattern, because of differences in the way that heat is transferred over wet and dry regions. Table 3 indicates that all the simulations reproduce a similar gradient pattern, but with different magnitudes. The simulations using the Emanuel scheme generally produce surface heat fluxes that match more closely with the observations, with ISEIN performing the best over the Guinean coast and IMEIN performing the best over the Sahel and northern Africa.

Since the surface heat fluxes are influenced by net radiation, we present the spatial distributions of the ratio of latent and sensible heat fluxes to net radiation for the summer season (JJA) (Fig. 9). Presentations of these ratios give insight into model performances in simulating surface heat fluxes as well as energy partitioning. Generally, BSEIN overestimates the ratio of the latent heat flux across the Guinean coast and Sahel, which correspond to regions characterized by strong wet bias. On the other hand, BSEIN underestimates the ratio of sensible heat flux over northern Africa even though sensible heat flux itself is overestimated (not shown) because of the positive bias in surface net radiation over this region. It reflects wrong partitioning of surface heat fluxes,
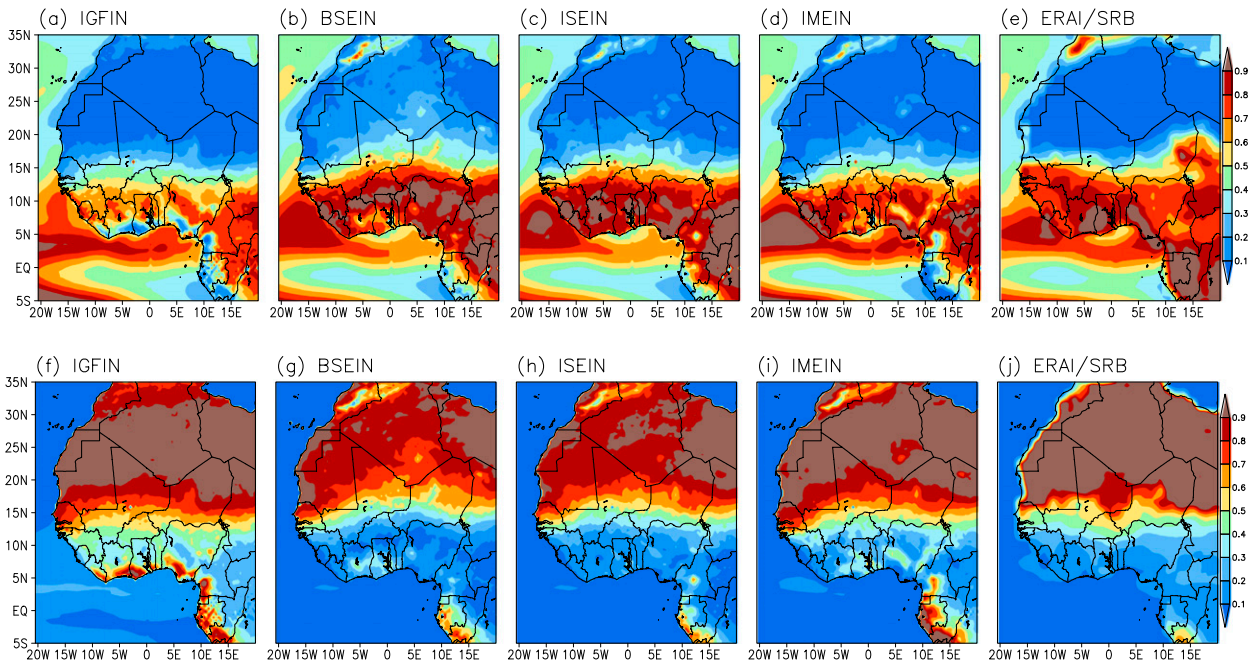

FIG. 9. Spatial distribution of the ratio of (top) latent and (bottom) sensible heat fluxes to net radiation for the summer season (JJA) from the four experiments and ERA-Interim (heat fluxes) and SRB observations (radiation) averaged over the period 1989–98.
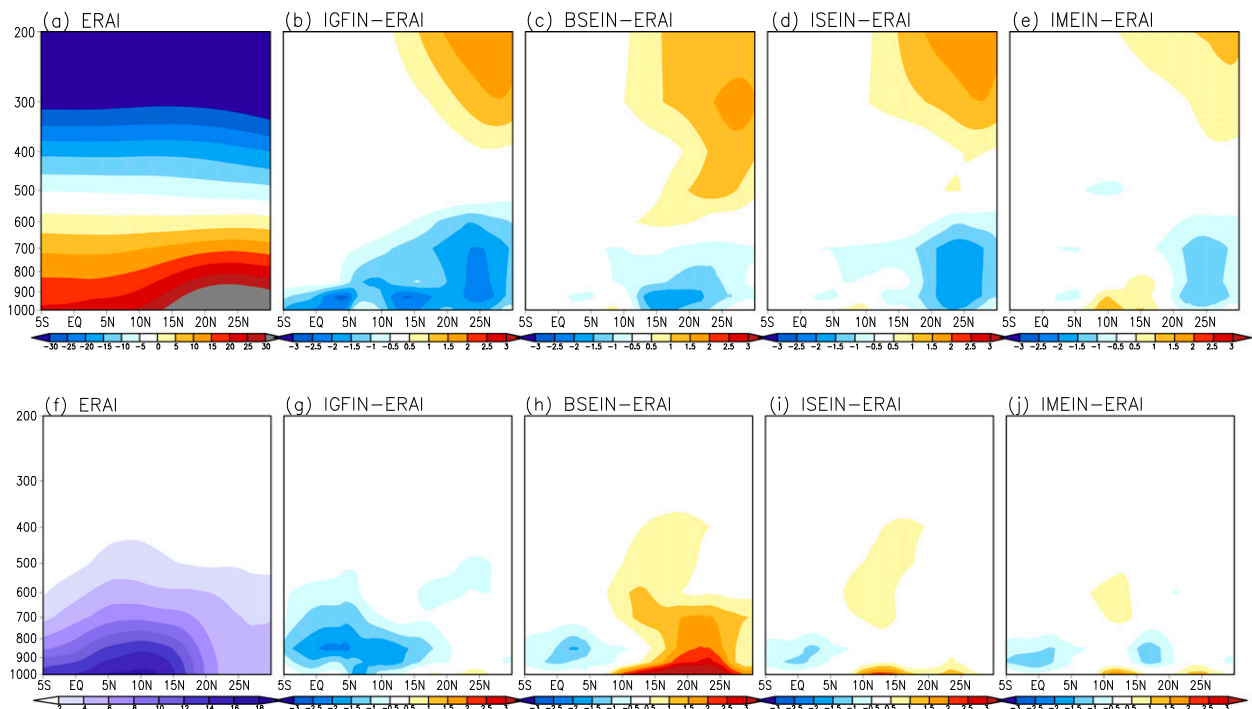
FIG. 10. Vertical cross section of JJA mean (top) temperature (°C) and (bottom) specific humidity (g kg^{-1}) averaged over 10°W–10°E from (a),(f) ERA-Interim, and the differences between the four experiments and ERA-Interim for (b)–(e) temperature and (g)–(j) specific humidity.

in addition to their systematic biases. Overall, the best performing model appears to be IMEIN in terms of adequate spatial distribution and absolute magnitudes of the latent and sensible heat fluxes.

Like our simulations, the S_BATS and S_CLM simulations by Steiner et al. (2009) exhibit substantial north–south gradients in latent and sensible heat fluxes, with S_CLM in better agreement with the reanalysis data (except for SH over the Guinean coast). Considering the results of Table 2 in Steiner et al. (2009), the coupling of CLM3 with RegCM3 leads to improvement in simulated surface heat fluxes compared to BATS, but not in surface radiation. This inconsistency is reflected in significant overestimation of ground heat flux. Therefore, the RegCM3–CLM3 coupling does not appear to correctly represent the surface energy balance, even though it produces a better simulation of the WAM.

d. Vertical structure of temperature and humidity

Different behavior in the simulated cloudiness (section 3b) and surface energy balance (section 3c) directly affects the simulated temperature and humidity. Figure 10 presents the vertical structure of the zonally averaged (10°W–10°E) temperature and specific humidity from ERA-Interim and the patterns of the bias in the four simulations. First, ERA-Interim shows the northward

increase and vertical decrease pattern in temperature. The simulations reproduce reasonably well these gradients (not shown). However, all simulations also exhibit some bias relative to ERA-Interim, of varying magnitudes. Generally, cold biases are dominant at lower altitudes while warm biases are dominant in the upper levels. Also, the biases tend to become larger moving from south to north. The IGFIN simulation shows the strongest cold bias across all latitudes, consistent with IGFIN also exhibiting the lowest surface net radiation. In contrast, the BSEIN simulation shows the strongest warm bias in the upper troposphere. The IMEIN simulation appears to have the smallest temperature bias at all latitudes and altitudes.

Considering the specific humidity distribution, it decreases with height as temperature does, but the latitudinal displacement is rather opposite. The patterns in the bias of simulated specific humidity reflect the deficiencies of rainfall seen in Fig. 2. IGFIN shows the largest negative bias of specific humidity among other simulations; thus, cooler and drier conditions in the low atmosphere hinder appropriate convective activity. On the other hand, BSEIN is characterized by excessive moisture, which is in line with strong wet bias of rainfall simulation. In spite of the cold bias in temperature, such excessive moisture can lead to the higher moist
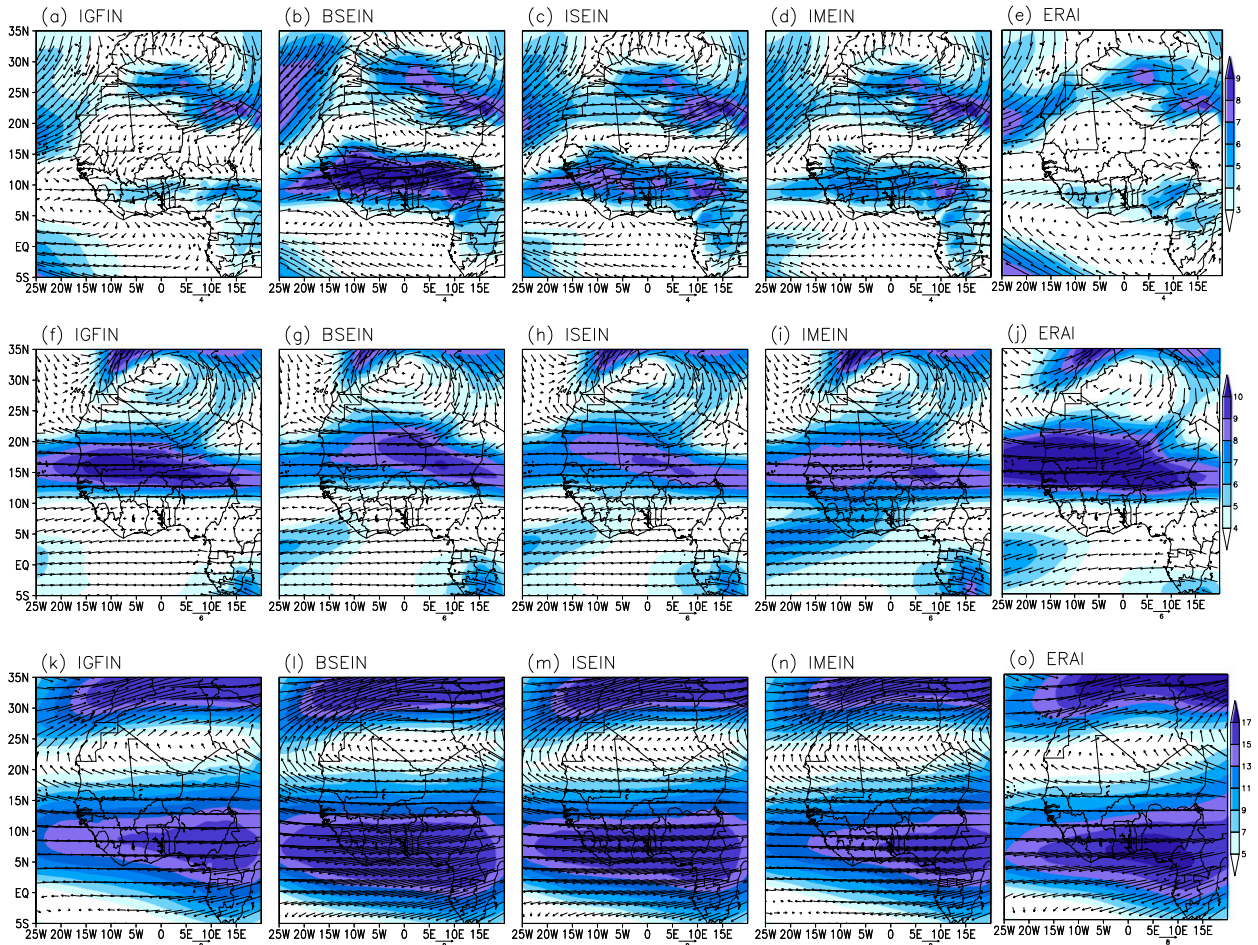
FIG. 11. Spatial distribution of wind vectors at (top) 850, (middle) 600, and (bottom) 200 hPa averaged for the month of August from the four simulations and ERA-Interim. Here, color shading indicates the magnitude of the wind (m s^{-1}).

static energy, and this results in an increase of CAPE forming a favorable environment for inducing convection (Eltahir 1998; Findell and Eltahir 2003). Again, the IMEIN simulation shows the best performance in the vertical structure of specific humidity.

e. Large-scale circulation

Finally, we assess the model performances with respect to the large-scale circulation at three atmospheric levels to provide useful information about the simulated three-dimensional dynamical structures of the WAM system.

Figure 11 presents the wind vectors at 850, 600, and 200 hPa averaged for the month of August derived from the four simulations forced by ERA-Interim and the ERA-Interim itself. To reduce the smoothing or cancelation effect of the dynamic fields, we provide the results for only August (peak timing of WAM) rather than JJA mean in this section.

At 850 hPa, ERA-Interim shows that the westerly monsoon flow is prevailing over the Guinean coast and Soudano-Sahelian region, which carries moist air from the Atlantic Ocean. Winds are predominantly northeasterly past the western Sahara and Mauritania in the northwestern corner of the domain, along the flank of the North Atlantic anticyclonic flow, while an easterly flow stretches across the Saharan low thermal region.

The simulations all reproduce these major features of the low-level circulation, but significant discrepancies are observed in the simulated westerly monsoon flow over the Guinean region. Compared to ERA-Interim, the IGFIN simulation tends to produce less moisture influx due to a weaker monsoonal flow while the others simulations (with the Emanuel scheme) produce stronger advection of moisture due to a stronger westerly flow. In particular, the BSEIN simulation exhibits a much stronger westerly flow than shown in either the ERA-Interim or the other simulations, with the maximum wind speed situated farther north. This result relates well to the spatial distribution of rainfall
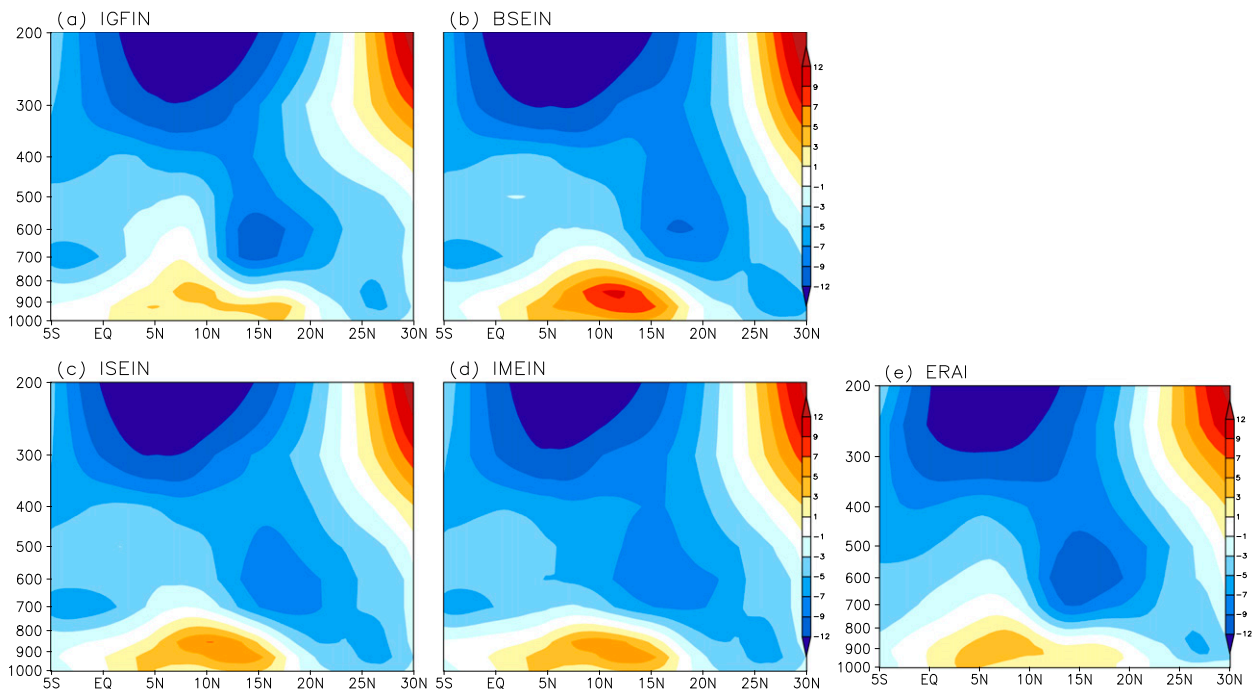
FIG. 12. Vertical cross section of zonal wind (m s^{-1}) averaged from 10°W to 10°E for the month of August from (a)–(d) the four experiments and (e) ERA-Interim. The vertical axis is in units of hectopascals (hPa).

simulated by BSEIN characterized by a strong wet bias over the Soudano-Sahelian region and a dry bias over the Guinean coast. Regarding the circulation to the west of the coast of Senegal, BSEIN, ISEIN, and IMEIN show flows from cyclonic circulation linked while high rainfall is simulated off the West African coast.

At 600 hPa, strong easterly flow related to the African easterly jet (AEJ) is the most dominant feature. Although the simulated flow patterns at this altitude capture the major characteristics of ERA-Interim, none of the simulations using the Emanuel scheme reproduces the exact position and strength of maximum easterly flow as seen in ERA-Interim. All simulations underestimate the strength of the easterly flow and the location of maximum flow appears to be shifted eastward in the simulations, lacking the broad maximum across the Sahel shown in ERA-Interim. Unlike other variables displayed in section 3a–d, IGFIN shows the best performance in capturing not only the position of the maximum but also the corresponding strength.

Lastly, at 200 hPa, there are strong easterlies in a zonally broad band extending across the Guinean region and strong westerlies along the northern boundary of the domain. These strong flows in the upper troposphere and the resultant upper-level divergence are consistent with the simulated low-level convergence, which dynamically supports ascent of warm and moist air from

near the surface (see Fig. 13). The simulations appear to reproduce these two major features of upper-level flow. However, the BSEIN and ISEIN simulate easterlies that are too strong compared to ERA-Interim, while the IGFIN and IMEIN have the location of maximum eastward flow shifted eastward.

Figure 12 presents the vertical structure of the zonal wind averaged from 10°W to 10°E for the month of August. The vertical structure shows a rather stratified behavior of the atmospheric circulation with three major components. The westerly flow prevailing up to 800 hPa describes the monsoon flow and the easterlies centered around 600 and 200 hPa describe the AEJ and tropical easterly jet (TEJ), respectively.

The westerly monsoon flow prevails between the equator and 20°N. The intensity and position of the monsoon flow is one important factor determining the magnitude and the spatial distribution of rainfall. Compared to ERA-Interim, Fig. 12 shows that the simulations generally tend to shift the extent of the westerly monsoon flow northward, locating the maximum flow around 10°–15°N rather than closer to the Guinean coast (around 5°–10°N). Consistent with the simulated wind fields at 850 hPa (Fig. 11), the BSEIN simulation shows a positive bias in the strength of the monsoon compared to ERA-Interim. The other simulations produce monsoon flow with a comparable strength to the reanalysis.
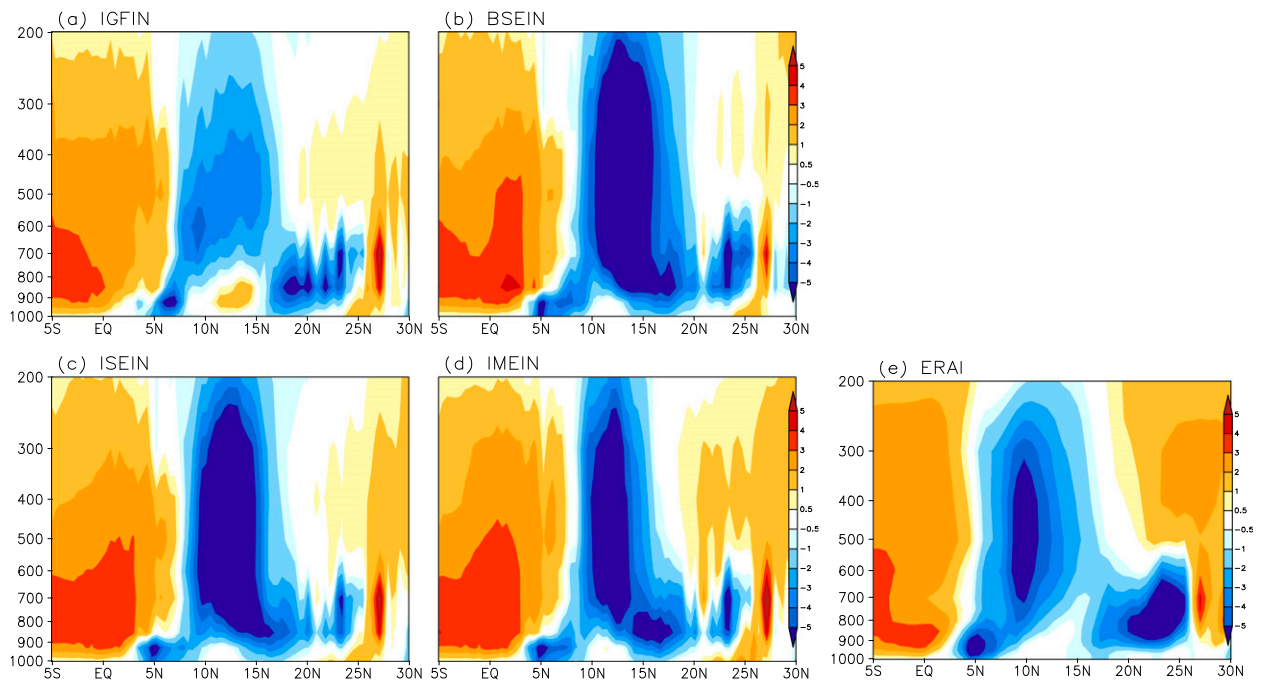
FIG. 13. As in Fig. 12, but for ω (pressure velocity; 10^5 hPa s^{-1}).

The AEJ is also considered a key element of the West African atmospheric flow. It is attributed to the strong baroclinicity resulting from the strong meridional gradient of surface temperature and moisture between the Sahara and equatorial Africa (Newell and Kidson 1984; Cook 1999; Thorncroft et al. 2003; Thorncroft and Blackburn 1999). The simulations all reasonably reproduce the existence of the AEJ centered around 600 hPa and 15°N. However, ISEIN and IMEIN produce an AEJ with a somewhat distorted shape and with less intensity than in the reanalysis. The BSEIN simulation also exhibits a northward-shifted core, which is induced by error in the monsoon flow since an overly strong and northward monsoon flow tends to push the AEJ farther northward as well. It is interesting to note that the IGFIN, which performs poorly in simulating the monsoon rainfall in the model, performs best in reproducing the magnitude of the AEJ.

Regarding the TEJ, the simulations all reproduce the strength, vertical depth, and latitudinal location reasonably well compared to ERA-Interim. There is some overestimation of the strength of the easterly in the TEJ core within BSEIN, which is consistent with the overestimation of the strength of the monsoon circulation. In general, a northward shift of the AEJ and the intensification of the TEJ shown in the BSEIN simulation are found in the observed behavior during abnormally wet period over Sahel (Gu et al. 2004; Grist and Nicholson 2001; Newell and Kidson 1984).

Figure 13 presents the vertical cross section of ω (pressure velocity) averaged from 10°W to 10°E for the month of August. The vertical motion shows strong sensitivity to the choice of convection scheme, with greater similarities among the BSEIN, ISEIN, and IMEIN simulations than between IGFIN and any one of the Emanuel scheme simulations. Despite differences in the simulated magnitude and shape, three positions of strong ascending motion are reproduced in the regional simulations when compared to the reanalysis. The first is located at 5°N along the coastline of the Gulf of Guinea. The vertical depth of this ascending motion is very shallow, and all simulations tend to underestimate its magnitude. This result is consistent with the underestimation of rainfall shown by all simulations along the coastal Guinean region. The central and primary region of ascending motion is located around 10°N with a depth extending all the way to 200 hPa. The simulations show a diversity of performances in simulating this rising core, which is related to convective activity. Compared to the reanalysis, BSEIN and ISEIN exhibit a northward displacement of the vertical motion, with a stronger and broader region of maximum ascent. This bias in the BSEIN and ISEIN simulations relative to the reanalysis is consistent with the excessive rainfall in these simulations over the Soudano-Sahel region. In IMEIN, the region of deep ascent becomes narrower and weaker, more closely resembling the reanalysis. The rising motion shown in the reanalysis between 15° and 25°N is
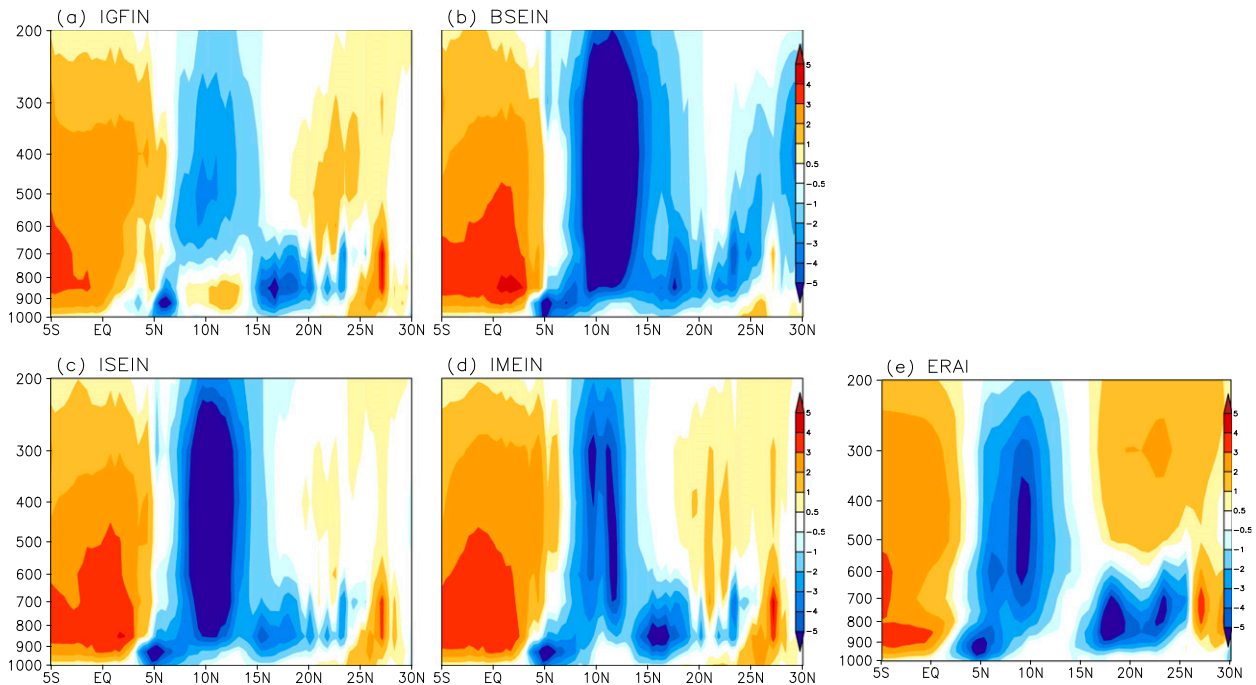
FIG. 14. As in Fig. 13, but for September.

characterized by dry convection in the Saharan heat low (Nicholson 2009; Sylla et al. 2011; Redelsperger et al. 2002). The simulations all underestimate the strong ascent in this location. In general, the IGFIN simulation systematically underestimates ascent, which is consistent with the weaker convective activity simulated by the Grell convection scheme compared to the Emanuel scheme.

The pressure velocity in September again clearly shows the different performances of the simulations implementing the default and modified Emanuel schemes (Fig. 14). The ERA-Interim shows the reduced magnitude and extent of ascending motion, indicating that the WAM enters the retreat phase. The IMEIN simulaton demonstrates skill at capturing this evolution feature. The central and primary ascending motion becomes weaker in September than in August, which is consistent with ERA-Interim. On the other hand, the BSEIN and ISEIN simulations still maintain strong ascending motion in September, failing to capture the WAM retreat at the correct time. Figure 14 clearly demonstrates how well the IMEIN simulates this key feature of the WAM compared to any of the other simulations shown in this study.

4. Summary and conclusions

This paper presents results of simulation using the MIT regional climate model (MRCM). The MRCM is built on the RegCM3, but with several significant improvements. First, MRCM couples RegCM3 to the IBIS land surface scheme with the addition of a new irrigation scheme. Other important features of MRCM are the introduction of new schemes for convective cloud cover and convective rainfall autoconversion, a modified representation of the nocturnal planetary boundary layer height, and a modified representation of large-scale cloud cover within the mixed boundary layer. This work evaluates the performance of MRCM in simulating features of the West African monsoon (WAM), with particular emphasis on the impact of the choices of land surface scheme and convection scheme.

The results of the numerical experiments presented here indicate that simulation of the WAM exhibits strong sensitivity to the choice of both land surface scheme and convection scheme. The improvement in the spatial and temporal distribution of rainfall in simulations using IBIS, rather than the default BATS scheme, is significant. In addition, the modifications incorporated within MRCM with respect to convective cloud cover, autoconversion, and boundary layer characteristics significantly improved the simulation of rainfall.

First, this study shows that using MRCM with the Emanuel convection scheme with all modifications, including those introduced to the representation of clouds and rainfall formation, produces the best overall performance with respect to simulation of rainfall. This is especially true for the spatial distribution, monthly evolution, and magnitude of monsoonal rainfall compared to observations. On the other hand, the Grell

convection scheme tends to underestimate rainfall over western Africa while the default version of RegCM3 using the Emanuel scheme significantly overestimates rainfall, which is consistent with previous studies (Steiner et al. 2009).

Second, the simulated surface energy budget is also shown to be sensitive to the choices of the land surface and convection schemes. The choice of land surface scheme appears to have a greater influence on net radiation. In this respect, simulations using IBIS are shown to be more accurate compared to observations over West Africa than simulations using other land surface schemes. The overestimation in net radiation exhibited by BATS is shown to be strongly influenced by an underestimation of surface albedo in this scheme.

The MRCM simulations, using IBIS and the Emanuel convection scheme with all new modifications, exhibit the best overall performance with respect to the spatial distributions and magnitudes of surface net radiation and turbulent heat flux partitioning. The Grell scheme seems to underestimate the net radiation and latent heat flux, which leads to the underestimation of rainfall. Using the default version of the Emanuel scheme together with BATS leads to an overestimation of both net radiation and latent heat flux and thus a substantial wet bias in simulated rainfall.

Finally, it is shown that the MRCM is capable of reproducing the main features of the large-scale circulation of the WAM, including a low-level westerly monsoonal flow, midlevel African easterly jet, and high-level tropical easterly jet. In particular, MRCM demonstrates a significant skill at capturing seasonal intensification and decay of dynamic fields when compared to other simulations shown in this work. The results presented here suggest a significant potential for MRCM as a tool to investigate land–atmosphere interactions over West Africa, such as the impact of land use changes resulting from irrigation.

REFERENCES

Abiodun, B. J., and Coauthors, 2012: Modeling the impact of reforestation on future climate in West Africa. *Theor. Appl. Climatol.,* **110,** 77–96, doi:10.1007/s00704-012-0614-1.

Adler, R. F., and Coauthors, 2003: The version 2 Global Precipitation Climatology Project (GPCP) monthly precipitation analysis (1979–present). *J. Hydrometeor.,* **4,** 1147–1167, doi:10.1175/1525-7541(2003)004<1147:TVGPCP>2.0.CO;2.

Afiesimama, E. A., J. S. Pal, B. J. Abiodum, W. J. Gutowski, and A. Addedoyin, 2006: Simulation of West African monsoon using the RegCM3. Part I: Model validation and interannual variability. *Theor. Appl. Climatol.,* **86,** 23–37, doi:10.1007/s00704-005-0202-8.

Cook, K. H., 1999: Generation of the African easterly jet and its role in determining West African precipitation. *J. Climate,* **12,** 1165–1184, doi:10.1175/1520-0442(1999)012<1165:GOTAEJ>2.0.CO;2.

Dickinson, R. E., A. Henderson-Sellers, and P. J. Kennedy, 1993: Biosphere–Atmosphere Transfer Scheme (BATS) version 1 as coupled to the NCAR Community Climate Model. NCAR Tech. Note NCAR/TN-387+STR, 72 pp., doi:10.5065/D67W6959.

Eltahir, E. A. B., 1998: A soil moisture–rainfall feedback mechanism. 1. Theory and observations. *Water Resour. Res.,* **34,** 765–776, doi:10.1029/97WR03499.

——, and C. Gong, 1996: Dynamics of wet and dry years in West Africa. *J. Climate,* **9,** 1030–1042, doi:10.1175/1520-0442(1996)009<1030:DOWADY>2.0.CO;2.

Emanuel, K. A., and M. Zivkovic-Rothman, 1999: Development and evaluation of a convection scheme for use in climate models. *J. Atmos. Sci.,* **56,** 1766–1782, doi:10.1175/1520-0469(1999)056<1766:DAEOAC>2.0.CO;2.

Findell, K. L., and E. A. B. Eltahir, 2003: Atmospheric controls on soil moisture–boundary layer interactions. Part I: Framework development. *J. Hydrometeor.,* **4,** 552–569, doi:10.1175/1525-7541(2003)004<0552:ACOSML>2.0.CO;2.

Flaounas, E., S. Bastin, and S. Janicot, 2010: Regional climate modeling of the 2006 West African monsoon: Sensitivity to convection and planetary boundary layer parameterization using WRF. *Climate Dyn.,* **36,** 1083–1105, doi:10.1007/s00382-010-0785-3.

Fontaine, B., S. Louvet, and P. Roucou, 2008: Definition and predictability of an OLR-based West African monsoon onset. *Int. J. Climatol.,* **28,** 1787–1798, doi:10.1002/joc.1674.

Fritsch, J. M., and C. F. Chappell, 1980: Numerical prediction of convectively driven mesoscale pressure systems. Part I: Convective parameterization. *J. Atmos. Sci.,* **37,** 1722–1733, doi:10.1175/1520-0469(1980)037<1722:NPOCDM>2.0.CO;2.

Gallee, H., and Coauthors, 2004: A high-resolution simulation of a West African rainy season using a regional climate model. *J. Geophys. Res.,* **109,** D05108, doi:10.1029/2003JD004020.

Gianotti, R. L., 2012: Regional climate modeling over the Maritime Continent: Convective cloud and rainfall processes. Ph.D. dissertation, Massachusetts Institute of Technology, 306 pp.

——, and E. A. B. Eltahir, 2014a: Regional climate modeling over the Maritime Continent. Part I: New parameterization for convective cloud fraction. *J. Climate,* **27,** 1488–1503, doi:10.1175/JCLI-D-13-00127.1.

——, and ——, 2014b: Regional climate modeling over the Maritime Continent. Part II: New parameterization for autoconversion of convective rainfall. *J. Climate,* **27,** 1504–1523, doi:10.1175/JCLI-D-13-00171.1.

——, D. Zhang, and E. A. B. Eltahir, 2012: Assessment of the Regional Climate Model version 3 over the Maritime Continent using different cumulus parameterization and land surface schemes. *J. Climate,* **25,** 638–656, doi:10.1175/JCLI-D-11-00025.1.

Giorgi, F., and Coauthors, 2012: RegCM4: Model description and preliminary tests over multiple CORDEX domains. *Climate Res.,* **52,** 7–29, doi:10.3354/cr01018.

Grell, G. A., 1993: Prognostic evaluation of assumptions used by cumulus parameterizations. *Mon. Wea. Rev.,* **121,** 764–787, doi:10.1175/1520-0493(1993)121<0764:PEOAUB>2.0.CO;2.

——, J. Dudhia, and D. R. Stauffer, 1994: A description of the fifth generation Penn State/NCAR Mesoscale Model (MM5). NCAR Tech. Note NCAR/TN-398+STR, 121 pp., doi:10.5065/D60Z716B.

Grist, J. P., and S. E. Nicholson, 2001: A study of the dynamic factors influencing the rainfall variability in the West African Sahel. *J. Climate,* **14,** 1337–1359, doi:10.1175/1520-0442(2001)014<1337:ASOTDF>2.0.CO;2.

Gu, G., R. F. Adler, G. J. Huffman, and S. Curtis, 2004: African easterly waves and their association with precipitation. *J. Geophys. Res.,* **109,** D04101, doi:10.1029/2003JD003967.

Gupta, S. K., and Coauthors, 1999: A climatology of surface radiation budget derived from satellite data. *J. Climate,* **12,** 2691–2710, doi:10.1175/1520-0442(1999)012<2691:ACOSRB>2.0.CO;2.

Hernández-Diaz, L., R. Laprise, L. Sushama, A. Martynov, K. Winger, and B. Dugas, 2013: Climate simulation over CORDEX Africa domain using the fifth-generation Canadian Regional Climate Model (CRCM5). *Climate Dyn.,* **40,** 1415–1433, doi:10.1007/s00382-012-1387-z.

Holtslag, A. A. M., E. I. F. de Bruijin, and H. L. Pan, 1990: A high resolution air mass transformation model for short-range weather forecasting. *Mon. Wea. Rev.,* **118,** 1561–1575, doi:10.1175/1520-0493(1990)118<1561:AHRAMT>2.0.CO;2.

Im, E.-S., M. P. Marcella, and E. A. B. Elfatih, 2014: The impact of potential large-scale irrigation on the West African Monsoon and its dependence on location of irrigated area. *J. Climate,* **27,** 994–1009, doi:10.1175/JCLI-D-13-00290.1.

Kiehl, J. T., J. J. Hack, G. B. Bonan, B. A. Boville, B. P. Briegleb, D. L. Williamson, and P. J. Rasch, 1996: Description of NCAR Community Climate Model (CCM3). NCAR Tech. Note NCAR/TN-420+STR, 152 pp., doi:10.5065/D6WH2MZX.

Koster, R. D., and Coauthors, 2004: Regions of strong coupling between soil moisture and precipitation. *Science,* **305,** 1138–1140, doi:10.1126/science.1100217.

Le Barbé, L., T. Lebel, and D. Tapsoba, 2002: Rainfall variability in West Africa during the years 1950–90. *J. Climate,* **15,** 187–202, doi:10.1175/1520-0442(2002)015<0187:RVIWAD>2.0.CO;2.

Liebmann, B., and A. C. Smith, 1996: Description of a complete (interpolated) outgoing longwave radiation dataset. *Bull. Amer. Meteor. Soc.,* **77,** 1275–1277.

Marcella, M. P., 2012: Biosphere–atmosphere interactions over semi-arid regions: Modeling the role of mineral aerosols and irrigation in the regional climate system. Ph.D. dissertation, Massachusetts Institute of Technology, 282 pp.

——, and E. A. B. Eltahir, 2012: Modeling the summertime climate of southwest Asia: The role of land surface processes in shaping the climate of semiarid regions. *J. Climate,* **25,** 704–719, doi:10.1175/2011JCLI4080.1.

Mitchell, T. D., T. R. Carter, P. D. Jones, M. Hulme, and M. New, 2004: A comprehensive set of high-resolution grids of monthly climate for Europe and the globe: The observed record (1901–2000) and 16 scenarios (2001–2100). Tyndall Centre for Climate Change Research, Working Paper 55, 25 pp. [Available online at http://www.tyndall.ac.uk/content/comprehensive-set-high-resolution-grids-monthly-climate-europe-and-globe-observed-record-190.]

Newell, R. E., and J. W. Kidson, 1984: African mean wind changes between Sahelian wet and dry periods. *J. Climatol.,* **4,** 27–33, doi:10.1002/joc.3370040103.

Nicholson, S. E., 2009: A revised picture of the structure of the "monsoon" and land ITCZ over West Africa. *Climate Dyn.,* **32,** 1155–1171, doi:10.1007/s00382-008-0514-3.

Nikulin, G., and Coauthors, 2012: Precipitation climatology in an ensemble of CORDEX-Africa regional climate simulations. *J. Climate,* **25,** 6057–6078, doi:10.1175/JCLI-D-11-00375.1.

Pal, J. S., E. E. Small, and E. A. B. Eltahir, 2000: Simulation of regional-scale water and energy budgets: Representation of sub-grid cloud and precipitation processes within RegCM. *J. Geophys. Res.,* **105** (D24), 29 579–29 594, doi:10.1029/2000JD900415.

——, and Coauthors, 2007: The ICTP RegCM3 and RegCNET: Regional climate modeling for the developing world. *Bull. Amer. Meteor. Soc.,* **88,** 1395–1409, doi:10.1175/BAMS-88-9-1395.

Ramankutty, N., and J. Foley, 1999: Estimating historical changes in land cover: North American croplands from 1850 to 1992. *Global Ecol. Biogeogr.,* **8,** 381–396, doi:10.1046/j.1365-2699.1999.00141.x.

Redelsperger, J. L., A. Diongue, A. Diedhiou, J.-P. Ceron, M. Diop, J.-F. Gueremy, and J.-P. Lafore, 2002: Multi-scale description of a Sahelian synoptic weather system representative of the West African monsoon. *Quart. J. Roy. Meteor. Soc.,* **128,** 1229–1275, doi:10.1256/003590002320373274.

Solmon, F., N. Elguindi, and M. Mallet, 2012: Radiative and climatic effects of dust over West Africa, as simulated by a regional climate model. *Climate Res.,* **52,** 97–113, doi:10.3354/cr01039.

Steiner, A. L., J. S. Pal, S. A. Rauscher, J. L. Bell, N. S. Diffenbaugh, A. Boone, L. C. Sloan, and F. Giorgi, 2009: Land surface coupling in regional climate simulations of the West African monsoon. *Climate Dyn.,* **33,** 869–892, doi:10.1007/s00382-009-0543-6.

Sultan, B., and S. Janicot, 2000: Abrupt shift of the ITCZ over West Africa and intra-seasonal variability. *Geophys. Res. Lett.,* **27,** 3353–3356, doi:10.1029/1999GL011285.

Sylla, M. B., A. T. Gaye, J. S. Pal, G. S. Jenkins, and X. Q. Bi, 2009: High resolution simulations of West African climate using regional climate model (RegCM3) with different lateral boundary conditions. *Theor. Appl. Climatol.,* **98,** 293–314, doi:10.1007/s00704-009-0110-4.

——, E. Coppola, L. Mariotti, F. Giorgi, P. M. Ruti, A. Dell'Aquila, and X. Bi, 2010a: Multiyear simulation of the African climate using a regional climate model (RegCM3) with the high resolution ERA-Interim reanalysis. *Climate Dyn.,* **35,** 231–247, doi:10.1007/s00382-009-0613-9.

——, A. Dell'Aquila, P. M. Ruti, and F. Giorgi, 2010b: Simulation of the intraseasonal and the interannual variability of rainfall over West Africa with RegCM3 during the monsoon period. *Int. J. Climatol.,* **30,** 1865–1883, doi:10.1002/joc.2029.

——, F. Giorgi, P. M. Ruti, S. Calmanti, and A. Dell'Aquila, 2011: The impact of deep convection on the West Africa summer monsoon climate: A regional climate model sensitivity study. *Quart. J. Roy. Meteor. Soc.,* **137,** 1417–1430, doi:10.1002/qj.853.

Thorncroft, C. D., and M. Blackburn, 1999: Maintenance of the African easterly jet. *Quart. J. Roy. Meteor. Soc.,* **125,** 763–786, doi:10.1002/qj.49712555502.

——, and Coauthors, 2003: The JET2000 Project: Aircraft observations of the African easterly jet and African easterly waves. *Bull. Amer. Meteor. Soc.,* **84,** 337–351, doi:10.1175/BAMS-84-3-337.

Uppala, S. M., and Coauthors, 2005: The ERA-40 Re-Analysis. *Quart. J. Roy. Meteor. Soc.,* **131,** 2961–3012, doi:10.1256/qj.04.176.

Uppala, S., D. Dee, S. Kobayashi, P. Berrisford, and A. Simmons, 2008: Towards a climate data assimilation system: Status update of ERA-Interim. *ECMWF Newsletter,* No. 115, ECMWF, Reading, United Kingdom, 12–18.

Winter, J. M., and E. A. B. Eltahir, 2012: Modeling the hydro-climatology of the Midwestern United States. Part I: Current climate. *Climate Dyn.,* **38,** 573–593, doi:10.1007/s00382-011-1182-2.

——, J. S. Pal, and E. A. B. Eltahir, 2009: Coupling of Integrated Biosphere Simulator to Regional Climate Model version 3. *J. Climate,* **22,** 2743–2757, doi:10.1175/2008JCLI2541.1.

Xue, Y., and Coauthors, 2010: Intercomparison and analyses of the climatology of the West African Monsoon in the West African Monsoon Modeling and Evaluation Project (WAMME) first model intercomparison experiment. *Climate Dyn.,* **35,** 3–27, doi:10.1007/s00382-010-0778-2.

Zaroug, M. A. H., M. B. Sylla, F. Giorgi, E. A. B. Eltahir, and P. K. Aggarwal, 2013: A sensitivity study on the role of the swamps of southern Sudan in the summer climate of North Africa using a regional climate model. *Theor. Appl. Climatol.,* **113,** 63–81, doi:10.1007/s00704-012-0751-6.